11582 *Biochemistry* **2009,** *48,* 11582–11591
DOI: 10.1021/bi901709j

BIOCHEMISTRY
including biophysical chemistry & molecular biology
Article

Mechanism of Fibril Formation by a 39-Residue Peptide (PAPf39) from Human Prostatic Acidic Phosphatase[†]

Zhuqiu Ye,[‡,§] Kinsley C. French,[‡] Ludmila A. Popova,[∥] Igor K. Lednev,[∥] Maria M. Lopez,[‡] and George I. Makhatadze*[,‡,§]

[‡]*Center for Biotechnology and Interdisciplinary Studies,* [§]*Department of Biology, Rensselaer Polytechnic Institute, Troy, New York 12065, and* [∥]*Department of Chemistry, University at Albany, State University of New York, Albany, New York 12222*

Received October 2, 2009; Revised Manuscript Received November 4, 2009

ABSTRACT: PAPf39 is a 39-residue peptide fragment from the sequence of human prostatic acidic phosphatase. This peptide was shown to form amyloid-like fibrils, which have been implicated in facilitating semen-mediated HIV transmission. Thus understanding molecular details of PAPf39 peptide fibril formation may aid in elucidating the mechanism of how PAPf39 fibrils are involved in HIV etiology. To this end, the kinetics of PAPf39 peptide fibrillization was studied using a battery of biophysical methods (atomic force microscopy, ThT fluorescence assays, far-UV circular dichroism spectroscopy, deep-UV resonance Raman spectroscopy, size exclusion chromatography, analytical ultracentrifugation, and small-angle X-ray scattering). It has been shown that fibril formation follows a nucleation-dependent elongation mechanism. Several critical factors for fibrillization have been identified. It was shown that agitation and/or seeding is required for fibril formation at 37 °C and neutral pH, with an additional requirement of a salt concentration above ∼100 mM. Fibril formation by the PAPf39 peptide is inhibited by low pH or by low salt concentration at neutral pH. These observations suggest that the nucleation and fibrillization of the PAPf39 peptide are a tug-of-war between the interactions formed upon agitation and the electrostatic interactions, modulated by pH and salt concentration.

Amyloid fibrils are pathogenically associated with a range of debilitating human diseases such as Alzheimer's disease, Parkinson's disease, prion diseases, type II diabetes, cancer, and systemic amyloidosis, among others (*1*−*3*). Recently, proteins not linked to human diseases, such as the SH_3 domain of phosphatidylinositol 3-kinase, phosphoglycerate kinase, human muscle acylphosphatase, and hen egg white lysozyme (*4*−*8*), have also been found to form amlyloid-like fibrils *in vitro* under certain destabilizing conditions and possess inherently cytotoxic features similar to those of amyloidogenic proteins (*5*). It is now well accepted that amyloid formation is a generic property to all proteins and peptides (*9*).

Despite the distinct nature in sequence and structure of the precursor proteins, their fibrillar forms share some common features. For instance, they appear to have nonbranched fibrillar structures of 80−120 Å in diameter and indefinite lengths as determined by electron and atomic force microscopies (*10*). They possess cross-β structures, in which β-strands are perpendicular to and backbone hydrogen bonds are parallel to the fibril axis, as suggested by X-ray crystallography (*10*). Furthermore, they specifically bind dyes Congo Red (*11*) and Thioflavin T (*12*). It is also well established that amyloid fibril formation commonly follows a nucleation-dependent elongation mechanism (*9*, *13*), which is composed of a lag phase where a critical-size nucleus from either a destabilized or fragmented precursor is slowly built up, followed by a growth phase where the nucleus grows exponentially into amyloid fibrils and a final equilibrium phase where fibrils stop developing.

Recently, amyloid fibrils have been implicated in increasing semen-mediated HIV transmission by several orders of magnitude (*14*). Münch and colleagues discovered that a degradation product of human prostatic acidic phosphatase (PAP), corresponding to residues 248−286 in the PAP sequence, forms amyloid fibrils that appear to boost HIV infectivity in cultured cells (*14*). These findings have the potential to provide new therapeutics for the prevention of HIV transmission. A detailed understanding of the molecular mechanism of PAPf39 (PAP fragment of 39 amino acid residues) peptide fibril formation may aid in elucidating the mechanism of PAPf39 fibril involvement in HIV infection. In this work, we studied the kinetics of PAPf39 peptide fibril formation under defined conditions, as part of an ongoing investigation into the mechanism of fibril formation by the PAPf39 peptide. The effects of environmental factors such as agitation, seeding, pH, and ionic strength on the aggregation of this peptide were investigated using Thioflavin T (ThT) fluorescence assays, atomic force microscopy (AFM), circular dichroism (CD) and deep UV resonance Raman spectroscopies (DUVRR), size exclusion chromatography (SEC), analytical ultracentrifugation (AUC), and small-angle X-ray scattering (SAXS). We found that the kinetics of PAPf39 peptide fibril formation follows a typical nucleation-dependent elongation mechanism, with agitation, seeding, and high (100 mM NaCl) ionic strength promoting fibril formation and low ionic strength and low pH inhibiting this process.

MATERIALS AND METHODS

Solutions and Buffers. PBS buffer, 10 × phosphate-buffered saline stock (10 × PBS, in 1 L, contains 80 g of NaCl, 2.0 g of

[†]This work was supported by a grant from the New York State Foundation for Science, Technology, and Innovation (to G.I.M.) and in part by a National Science Foundation grant (CHE-0809525 to I.K.L.).

*Address correspondence to this author at the Center for Biotechnology and Interdisciplinary Studies, Rensselaer Polytechnic Institute. Phone: (518) 276-4417. Fax: (518) 276-2955. E-mail: makhag@rpi.edu.

 Published on Web 11/10/2009 © 2009 American Chemical Society

KCl, 14.4 g of Na_2HPO_4, 2.4 g of KH_2PO_4, and 2 g of NaN_3 preservative, pH 7.4), was first prepared and sterilized by filtration through a 0.22 μm Millipore HV filter. Ten × PBS stock was diluted to a 1 × PBS working solution before each experiment. PB buffer, 0.2 M phosphate buffer (10 × PB, in 1 L, contains 4.42 g of sodium phosphate monobasic, 22.51 g of sodium phosphate dibasic heptahydrate, and 2 g of NaN_3 preservative, pH 7.4), was prepared and sterilized by filtration through a 0.22 μm Millipore HV filter. Ten × PB stock was diluted into 1 × PB (20 mM) working solution before each experiment. 2% Ac = 2% (v/v) acetic acid in Milli-Q water.

Peptide Synthesis and Purification. PAPf39 peptide corresponding to residues 248−286 of the sequence of human prostatic acidic phosphatase (NH_2-GIHKQKEKSRLQGGVLVNEILN-HMKRATQIPSYKKLIMY-COOH) was synthesized using standard Fmoc chemistry at the Penn State College of Medicine Macromolecular Core Facility. This peptide sequence is the same sequence as used previously by Münch et al. (*14*). The peptide was purified on C18 reverse-phase HPLC using a 0% to 100% gradient of either acetonitrile or methanol in the presence of 0.05% trifluoroacetic acid (TFA). The fractions containing the peptide were pooled and subjected to three cycles of lyophilization and resuspension in Milli-Q water to remove residual TFA. The molecular mass of the peptide (4551 Da) and the absence of residual TFA in the sample were confirmed by mass spectroscopy (Bruker Ultraflex III MALDI TOF/TOF). Peptide concentration was determined using a molar extinction coefficient of 2980 M^{-1} cm^{-1} at 280 nm. PAPf39 peptide samples were freshly prepared before each experiment to minimize variations in the degree of aggregation that may lead to large experimental irreproducibilities.

Thioflavin T (*ThT*) *Fluorescence Assay*. ThT fluorescence assays were performed on FluoroMax or Fluorolog spectrofluorometers (HORIBA Jobin Yvone, Edison, NJ) at 37 °C. PAPf39 peptide samples were freshly prepared and incubated at 37 °C under various conditions. For Fluoromax experiments, at desired time intervals, 150 μL of incubated samples was withdrawn and mixed with 180 μL of 100 μM Thioflavin T (Sigma-Aldrich) and 870 μL of 1 × PBS (pH 7.4) to a total volume of 1200 μL in a quartz cuvette. For Fluorolog experiments, at desired time intervals, 50 μL of incubated samples was withdrawn and mixed with 60 μL of 100 μM Thioflavin T (Sigma-Aldrich) and 440 μL of 1 × PBS (pH 7.4) to a total volume of 550 μL in a quartz cuvette. Note that the ratio of peptide to ThT was kept the same in the two experiments using different spectrofluorometers. After being stirred for 30 s, the samples were subjected to a wavelength scan and/or time scan. For a wavelength scan, ThT was selectively excited at 440 nm, and the emission spectrum was monitored from 450 to 550 nm. For a time scan, the changes in ThT fluorescence intensity at 482 nm (emission maximum) after excitation at 440 nm were recorded and averaged for 90 s intervals. ThT alone in PBS without peptide was used as a blank. For seeding experiments, 2 mg/mL fresh PAPf39 peptide solution in PBS was agitated at 37 °C for 3−7 days to form fibrils. The preformed fibril solution was gently sonicated for 5 min, and a small portion of this solution (1%, 2%, and 3% (v/v)) was used to seed freshly prepared PAPf39 peptide solution for ThT fluorescence assays as described above.

Atomic Force Microscopy (*AFM*). AFM images were obtained at ambient temperature using a MFP-3DTM atomic force microscope from Asylum Research (Santa Barbara, CA), operating in tapping mode in air. Silicon cantilevers (AC240TS; Olympus) with a spring constant of 2 N/m and tip radius of less than 10 nm were used. Samples for AFM imaging were prepared in the following way: during the incubation, PAPf39 peptide samples were withdrawn at different time points and diluted 10−20-fold in the same incubation buffer (2% Ac, PB, or PBS). Aliquots of 20 μL of diluted samples were absorbed on a freshly cleaved mica surface, incubated for 15 min, and then gently rinsed with 4−5 mL of filtered Milli-Q water to remove extra sample layers. Samples were then air-dried overnight before imaging. Image analysis was performed with the Igor Pro 5.0 image processing package (WaveMetrics, Inc., Portland, OR).

Circular Dichroism (*CD*). Far-UV CD spectra were recorded on a Jasco-715 spectropolarimeter. PAPf39 peptide or fibril samples, at a peptide monomer concentration of 2 mg/mL, were prepared in PBS and diluted to 0.2 mg/mL for the peptide and 0.05 mg/mL for the fibrils. The spectra from 195 to 260 nm were collected in a 1 mm light path length circular quartz cuvette. For each spectrum, four wavelength scans were collected and averaged. The ellipicity of the peptide solution (θ) was corrected by subtracting the buffer baseline and converted to molar ellipicity using the equation $[\theta] = \theta M/(10lcn_r)$, where M is the molecular mass of the PAPf39 peptide (4551 Da), l is the light path length in centimeters, c is the peptide concentration in mg/mL, and $n_r = 39$ is the number of residues in the PAPf39 peptide.

Deep UV Resonance Raman (*DUVRR*) *Spectroscopy*. Deep UV Resonance Raman (DUVRR) spectra were recorded using a home-built spectrograph as described in detail elsewhere (*15*). Briefly, a 197 nm laser beam was focused into a spinning Suprasil NMR tube containing 100 μL of PAPf39 sample solution. Scattered radiation was collected in backscattering geometry, dispersed using a home-built double monochromator, and detected with a liquid nitrogen-cooled CCD camera (Roper Scientific). The accumulation time for a Raman spectrum was 10 min. GRAMS/AI (7.01) software was used for Raman spectroscopic data processing. The contribution of Suprasil, water, buffering salts, and internal standard was quantitatively subtracted. In hydrogen−deuterium exchange experiments, peptide fibrils were concentrated by centrifugation at 20000*g* for 30 min and then resuspended in either D_2O- or H_2O-based buffer composed of 10 mM sodium phosphate at pH 7.3. This procedure was performed twice to ensure significant H_2O-D_2O exchange.

Size Exclusion Chromatography (*SEC*). Size exclusion chromatography of the PAPf39 peptide was carried out on a Superdex 75 HR 10/30 size exclusion column (GE Healthcare) using an AKTA system (GE Healthcare). The system was preequilibrated with 20 mM sodium phosphate/300 mM NaCl buffer (pH 7.4). PAPf39 peptide samples were eluted using the same buffer at a flow rate of 0.5 mL/min. Aggregated peptide samples were centrifuged at 13000 rpm for 5 min to remove any precipitates prior to injections. Elution profiles were followed by monitoring the absorbance at 280 nm.

Equilibrium Analytical Ultracentrifugation (*AUC*). Equilibrium analytical ultracentrifugation experiments were performed on a Beckman XLA ultracentrifuge. A concentration of 2 mg/mL PAPf39 peptide prepared in three different solvents, 2% Ac, PB, and PBS, was centrifuged at 27 °C at three speeds (28000, 35000, and 40000 rpm) until the samples reached equilibrium. The samples were considered to be at equilibrium when there was no difference between three consecutive radial distribution scans, with a 6 h interval between each scan. Two-sector cells with an optical path length of 1.2 cm were used, and

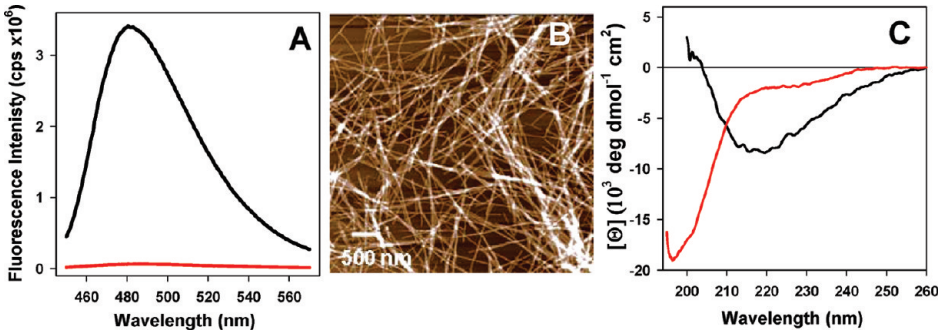

FIGURE 1: Characterization of PAPf39 peptide fibrils. Panel A: Thioflavin T (ThT) fluorescence spectra before (red line) and after (black line) binding to PAPf39 peptide fibrils. Panel B: Morphology of PAPf39 fibrils determined by atomic force microscopy (AFM). PAPf39 peptide fibrils were obtained by agitating 5 mg/mL PAPf39 peptide in PBS at 37 °C for 3 days. The AFM height image was taken in air at ambient temperature using tapping mode. Panel C: Far-UV CD spectrum of PAPf39 peptide fibrils (black line) and monomers (red line).

the absorbance was monitored at 288 nm. The sedimentation profiles were fitted to a single species model with nonideality according to the equation:

$$A(r) = I + A_0(r_0)e^{[(1-\bar{v}\rho)\omega^2/2RT]\mathrm{MW}(r^2-r_0^2)-BM(A_r-A_0)} \quad (1)$$

where $A(r)$ and $A_0(r_0)$ are the absorbances at each radial position and at r_0, respectively, I is the offset, $\bar{v}$ is the partial volume of the protein (0.753 cm^3/g calculated as described in ref *16*), ρ is the density of the buffer, ω is the angular velocity, T is the temperature in kelvin, R is the universal gas constant, MW is the molecular mass of the species present in solution, and B is the second virial coefficient. The sedimentation curves were fitted using nonlinear regression software (NLREG) as described by Makhatadze et al. (*16*).

Small Angle X-ray Scattering (*SAXS*). SAXS samples in three different solvents (2% Ac, PBS, and PB) at concentrations of 5 mg/mL PAPf39 peptide were prepared by agitation at 37 °C for 5 h. Samples were kept on ice prior to the experiment, and experiments were performed at room temperature on a Bruker Nanostar instrument with a HI-STAR detector and a 105 cm detector distance. All samples were measured in the same "boron-rich" capillary of 1.5 mm diameter with a 0.01 mm nominal wall thickness (Charles Supper Co.). The scattering profiles for each PAPf39 peptide solution and its corresponding buffer were collected for 1 h. No radiation damage was observed as measurements for different stock solutions gave similar results. The transmission normalized scattering profile of the buffer was subtracted from the peptide profile. The scattering profiles (intensity vs q, where q is the momentum transfer $q = 4\pi/\lambda \sin\theta$, 2θ is the scattering angle, and λ is the X-ray wavelength) were fitted using GNOM software by Svergun (*17*). The distribution function $p(r)$ of intramolecular atomic distances (D_{max} being the maximum intramolecular distance) was calculated as follows, using GNOM:

$$I(q) = \int_0^{D_{max}} p(r)\frac{\sin(qr)}{qr}\,dr \quad (2)$$

The radius of gyration R_g was also determined from the fit:

$$R_g^2 = \frac{\int_0^{D_{max}} p(r)r^2\,dr}{2\int_0^{D_{max}} p(r)^2\,dr} \quad (3)$$

In all cases, the parameter TOTAL, as defined by GNOM, was used as the main criteria for the determination of the goodness of the fit. It varied between 0.7 and 0.9 for 2% Ac and PBS, suggesting either a reasonable or good solution to eq 2. However, the scattering profile in PB was not possible to fit to a monodisperse model, and thus the data are not included here.

RESULTS AND DISCUSSION

PAPf39 Fibril Structure Characterization. Thioflavin T is a fluorescent probe that is believed to specifically interact with the cross-β structure common to amyloid fibrils (*12*, *18*). The binding of ThT to amyloid fibrils is independent of the amino acid sequence of the proteins and peptides. Only the fibrillar forms of a protein or peptide, not β-sheet domains in native proteins, give significant fluorescence with ThT. In the absence of amyloid fibrils, ThT has a relatively low emission maximum at 438 nm (after excitation at 350 nm). Binding of ThT to amyloid fibrils gives rise to a new excitation maximum at 440 nm with a new emission maximum at 482 nm and dramatic enhancement in fluorescence intensity. Figure 1A compares the fluorescence spectrum of ThT in the presence of PAPf39 peptide fibrils with that of free ThT alone. It can be seen that, in the presence of PAPf39 peptide fibrils, ThT shows a large increase in fluorescence intensity from 450 to 550 nm, as compared to ThT alone, indicating the presence of fibrils with a cross-β structure. This suggests that PAPf39 fibrils interact with ThT in a manner similar to that of other amyloid-forming sequences (*12*, *18*) and provides a useful tool to measure the kinetics of PAPf39 peptide fibril formation.

Atomic force microscopy (AFM) is a powerful tool that has been widely used to examine morphological changes and kinetics of amyloid fibril formation (*19*), including the amyloid-β peptide in Alzeimer's disease, α-synuclein in Parkinson's diseases, etc. (*20*−*24*). We used this method (see actual description of the methodology in the Materials and Methods section) to characterize the PAPf39 peptide fibrils which were suggested by ThT binding experiments. As can be seen from the AFM image shown in Figure 1B, the PAPf39 peptide aggregates exhibit a well-defined, nonbranched fibrillar structure with an indefinite length, a structure that is indistinguishable from other amyloid fibrils (*1*, *10*).

Far-UV (190−260 nm) circular dichroism (CD) was applied to determine the secondary structure of monomeric PAPf39 peptide and its aggregated form. The α-helix, β-sheet, and random coil each display a characteristic far-UV CD spectrum (*25*). The spectrum of an α-helix shows two characteristic minima at 222 and 208 nm, whereas a β-sheet has a minimum around 218 nm, with a random coil lacking these features. As illustrated in Figure 1C, PAPf39 fibrils exhibit a typical β-sheet component

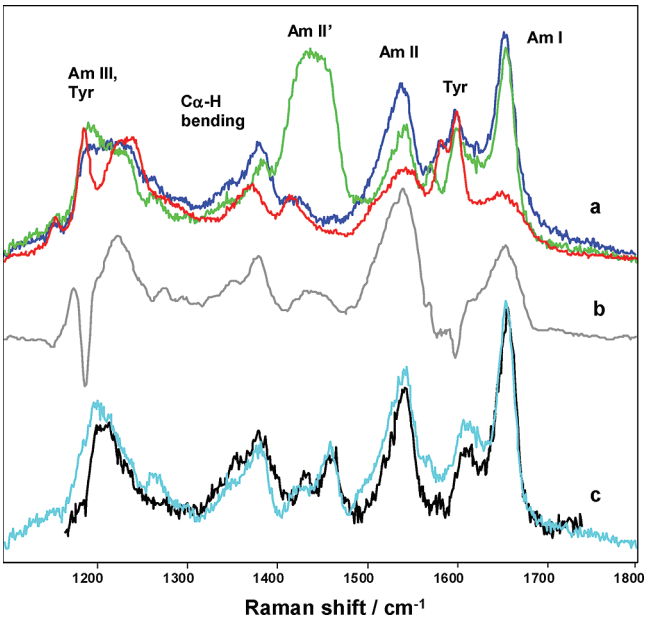

FIGURE 2: Hydrogen−deuterium exchange (HX) deep UV resonance Raman (DUVRR) spectra of PAPf39 fibrils. (a) Deep UV resonance Raman spectra of the PAPf39 monomer (red) and PAPf39 fibrils in H_2O (blue) and D_2O (green) and (b) representative DUVRR spectrum (*37*) of an average protein β-sheet in a globular protein (gray). (c) Comparison of DUVRR spectra of the fibrillar core formed by the PAPf39 peptide (blue) and by the fibrillar core of lysozyme (black). The latter was taken from ref *27*.

containing a single minimum at approximately 218 nm. The spectrum of the peptide monomer does not show characteristics of either an α-helix or β-sheet, indicating that PAPf39 monomer lacks a significant population of an ordered secondary structure. This suggests that the PAPf39 peptide undergoes a random coil to β-sheet transition upon fibril assembly, consistent with the results of AFM and ThT fluorescence experiments.

To obtain more detailed characterization of the secondary structure of PAPf39 fibrils, we used deep UV resonance Raman spectroscopy (DUVRR). DUVRR spectroscopy is a powerful tool for obtaining information on the secondary structure of both native and aggregated forms of proteins and peptides. The Raman signature of an amide chromophore is sensitive to the φ and ψ dihedral angles of a polypeptide chain, thus providing information about its secondary structure (*26*). Additionally, DUVRR spectroscopy is uniquely capable of differentiating between globular and fibrillar β-sheet secondary structures (*26*, *27*). Using a recently developed method (*26*) combining hydrogen−deuterium exchange and DUVRR spectroscopy, we looked for the Raman signature of the cross-β core, which is characteristic to amyloid fibrils (*15*, *26*). The rate of hydrogen−deuterium exchange is heavily diminished in strongly hydrogen-bonded structures due to shielding of exchangeable sites (*28*). This allows us to separate the spectral contributions of unordered aggregates from the stable hydrogen-bonded fibrillar cross-β core (*26*) using the spectral signatures of the deuterated fibrils and deuterated unordered peptides. In the DUVRR spectrum of deuterated PAPf39 fibrils (Figure 2a) the appearance of an amide II′ band is well-known to be a consequence of H-to-D isotope substitution. The ratio of intensities of amide II bands in hydrogenated and deuterated samples can be used as a measure of the degree of isotope substitution in the normalized spectra of fibrils. Using this method, the fraction of nonexchangeable core in PAPf39 fibrils is estimated to be 70−80%. A spectrum of deuterated Aβ1−40 peptide in an unordered conformation was used to represent a generic unordered peptide (*29*). This spectrum was subtracted from the spectrum of deuterated PAPf39 fibrils. The criterion of subtraction was to eliminate the amide II′ band that is only present in the deuterated peptide backbone. As a result, the Raman signature of the cross-β core of the PAPf39 fibrils was obtained (Figure 2c). The narrow and intense amide I and amide II bands in the fibrillar core spectrum indicate substantial presence of fibrillar-type β-sheet. The pure DUVRR spectrum of a β-sheet (averaged spectrum of β-sheet with no contribution from β-turns) extracted by means of least-squares regression from DUVRR spectra of 12 proteins with known secondary structures (*27*) is shown in Figure 2 for comparison. Overall, the DUVRR spectrum of PAPf39 fibrils resembles typical spectra of other amyloid fibrils such as the fibrillar core of lysozyme (*26*) (Figure 2c).

In summary, the fibrillar structure formed by the PAPf39 peptide was observed in AFM experiments. This fibrillar structure exhibits a β-structure as evidenced by far-UV CD spectroscopy and more specifically a cross-β core as confirmed by DUVRR spectroscopy. Together, with the enhancement of ThT fluorescence, these experiments strongly support the amyloid-like nature of PAPf39 peptide fibrils. These results confirm previous observations (*14*) and provide additional details on the similarity of PAPf39 fibrils with those observed for other proteins and peptides.

Role of Agitation and Concentration in PAPf39 Fibril Formation. After confirming the amyloid-like structure of PAPf39 peptide aggregates, we examined the factors required for peptide self-assembly into amyloid fibrils. It has been shown that the PAPf39 peptide readily forms fibrils upon agitation (*14*, *30*); however, a detailed characterization of the kinetics of this process was not reported. We first tested the effect of agitation and peptide concentration on the kinetics of fibril formation in PBS buffer. Peptide solutions with concentrations of 2 and 5 mg/mL were incubated at 37 °C with agitation for up to 100 h. Samples of the same concentrations were incubated at 37 °C without agitation to serve as controls. Aliquots from the incubated samples were withdrawn at defined time points and mixed with ThT, and the increase in fluorescence intensity of ThT was measured to monitor the kinetics of fibril formation. In the absence of agitation, both peptide concentrations examined displayed negligible changes in ThT fluorescence over a time course of 96 h (Figure 3A). This indicates that, without agitation, peptide fibril formation is very slow, if any. Conversely, the kinetics of peptide fibril formation upon agitation (Figure 3A) exhibits a strikingly different profile with an initial flat lag phase, followed by a steep growth phase and a final equilibrium phase. This sigmoidal curve, which is observed at both 2 and 5 mg/mL concentrations of PAPf39 peptide, is consistent with the characteristic nucleation-dependent elongation model found for most amyloidogenic proteins (*9*, *13*). The effect of peptide concentration is also consistent with a nucleation-dependent elongation model: a concentration of 2 mg/mL of the PAPf39 peptide has a distinct lag time of ~10 h whereas a concentration of 5 mg/mL has a reduced lag time of ~ 6 h (the errors of lag phase estimates from repeat experiments are on the order of ±1.5 h; see, e.g., Figure 3B). Furthermore, a higher peptide concentration (5 mg/mL) also corresponds to a faster growth

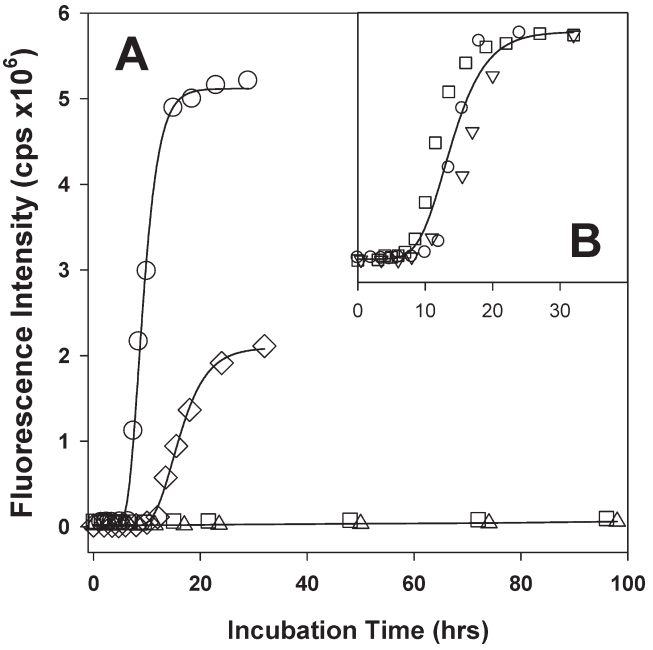

FIGURE 3: Effect of agitation on the kinetics of fibril formation of the PAPf39 peptide monitored by ThT fluorescence. Panel A: PAPf39 peptide at concentrations of 2 and 5 mg/mL was incubated in PBS at 37 °C with or without agitaion. Incubated samples were withdrawn at desired time points for a ThT binding assay. Triangles and squares represent 2 and 5 mg/mL PAPf39 peptide without agitation, respectively, while diamonds and circles represent 2 and 5 mg/mL PAPf39 peptide with agitation, respectively. Samples incubated without agitation did not show increase in ThT fluorescence even after 12 days (data not shown). Panel B: Comparison of three independent experiments at 2 mg/mL PAPf39 peptide with agitation to show the reproducibility of the data and associated errors. Solid lines are shown to guide the eye.

rate, i.e., a steeper slope of growth phase (Figure3A), again consistent with the above model.

To complement the ThT binding assay, AFM was used in parallel to examine the morphology of the amyloid fibrils and to identify possible intermediates formed at different times during PAPf39 peptide fibrillization. Figure 4A−I present the morphological changes of PAPf39 peptide incubated in PBS with agitation as visualized by AFM. Figure 4A at 0 h shows small spherical structures that appear to be present before incubation. Imaging of the mica surface or buffer alone ruled out the possibility that these structures are contaminants, artifacts from the mica surface, or originating from the buffer (data not shown). However, we cannot rule out the other experimental artifacts, such as AFM tip resolution, flattening effect during the drying process, and/or a high concentration of sample, that can exaggerate the size of these structures. The data from size exclusion chromatography (SEC) collected at 0 h of incubation suggest that the PAPf39 peptide is behaving as a monomer in solution (see Figure 8 below). It is also possible that these spherical structures could be small oligomeric artifacts that formed from the monomers in the process of preparing samples for AFM imaging. At 2 h (Figure 4B), a few bright spherical oligomers (as indicated by the red arrows) appear. The increase in brightness (i.e., height) suggests that these species are different than the spherical structures observed on the background of the same image or those observed at 0 h (see Figure 4A). After 5 h of agitation (see Figure 4C), abundant bright spherical oligomers with a height on the order of ~4 ± 1 nm (as indicated by the red arrow) are observed. A few short protofibrils with similar heights (as indicated by the black arrow) can also be observed at this time point. After 10 h of agitation, the spherical oligomers continue to elongate into short protofibrils as evidenced by the AFM image in Figure 4D,E. The head-to-tail junction of oligomers forms

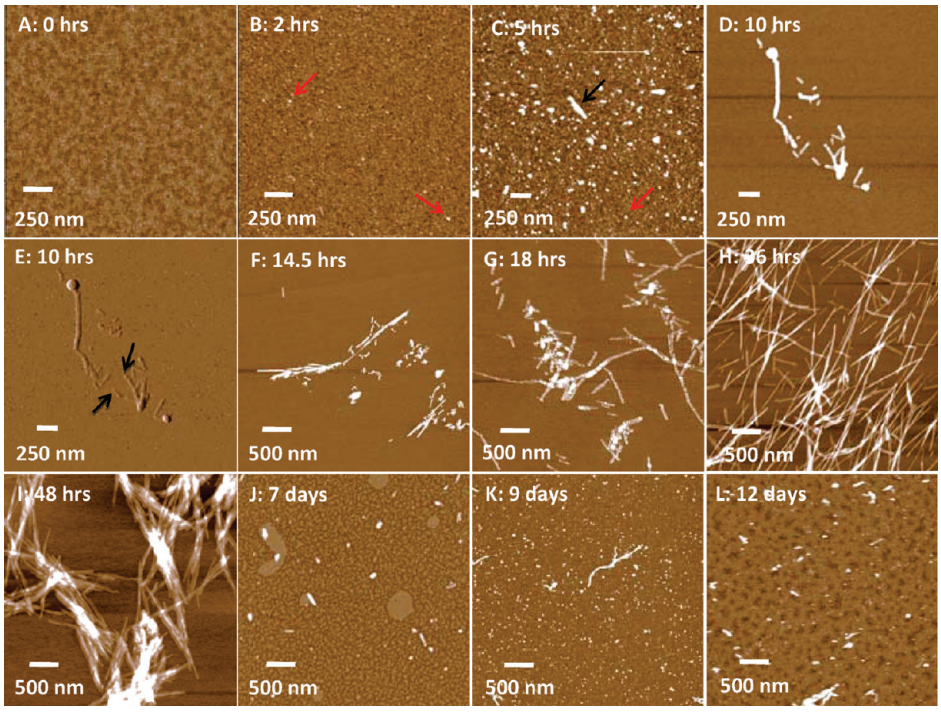

FIGURE 4: Effect of agitation on the kinetics of fibril formation of the PAPf39 peptide monitored by AFM. Panels A−I: 2 mg/mL PAPf39 peptide in PBS was agitated at 37 °C for up to 2 days. Panels D and E are the height and amplitude images of the same sample, while the rest are height samples. Panels J−L: 2 mg/mL of the PAPf39 peptide in PBS was incubated at 37 °C without agitation for up to 12 days as a control. Images were taken at the time points indicated on the figures. AFM height images were acquired using tapping mode in air.

bead-like protofibrils (as indicated by the black arrows), which indicate that these oligomers may be an obligate nucleus for protofibril formation. AFM images taken of samples incubated for 14.5 and 18 h (see panels F and G of Figure 4) show the presence of protofibrils with lengths varying from 300 nm to 1 μm, with some beginning to form even longer fibrils. Images shown in Figure 4G,H suggest that these protofibrils disappear over time and long fibrils become predominant after 36 and 48 h of incubation, respectively. At 36 h of incubation, the averaged length of fibrils varies from 1 to 4 μm with a predominant height of 7 ± 1 nm (~30%) or 11 ± 1 nm (~40%), although fibrils with a height of 4 ± 1 nm (~20%) and 16 ± 1 nm (~10%) are present as well. Importantly, not many small oligomeric structures are observed at this time point (see Figure 4H,I), suggesting their depletion due to fibrillization, which is consistent with the results of ThT binding assays performed on PAPf39 peptide samples in PBS that were agitated at 37 °C (see Figure 3A,B). A control experiment was performed using PAPf39 peptide samples incubated, without agitation, at 37 °C for up to 12 days (~290 h). As shown in Figure 4J−L, nonagitated PAPf39 peptide samples aggregate very slowly: AFM images of samples incubated for 7, 9, 10, and 12 days do not show an abundance of fibrils or large aggregates. In agreement with the ThT experiments shown in Figure 3A, this suggests that agitation is an important condition for PAPf39 peptide fibril formation, presumably via the agitation-induced fragmentation mechanism similar to that observed for β2-macroglobulin (*31*) and enhancement of interfacial interactions proposed for insulin (*32*).

To summarize, both ThT binding assays and AFM analysis support the notion that PAPf39 peptide fibril formation in PBS is dramatically accelerated by agitation and is concentration- and time-dependent. Aggregation upon agitation follows a nucleation-dependent elongation model. The slow formation of the oligomeric intermediate (with an estimated height of 4 ± 1 nm) explains the lag time: no significant aggregation is observed until a critical population of these nucleating species is established. After ~10 h, these spherical oligomers begin to elongate into short protofibrils. Consistent with AFM data, ThT binding assays demonstrate that an increase in ThT binding begins at ~10 h, suggesting the transition of oligomeric intermediates to protofibrils and fibrils with cross-β structures. At the final stage, long fibrils of indefinite length and varied heights develop.

Effect of Seeding on PAPf39 Peptide Fibril Formation. We have shown that PAPf39 peptide fibril formation appears to follow a typical nucleation-dependent elongation mechanism (*2*), with a nucleation process occurring during lag phase, followed by a fibril elongation process during exponential growth phase. It is known that seeding can eliminate the lag phase by providing nuclei for fibril growth (*13*). To further investigate the mechanism of PAPf39 peptide fibril formation, we compared the effects of seeding and agitation. As shown above (see Figure 3A) and also in Figure 5B (data points after 32 h are omitted for the clarity), PAPf39 peptide fibril formation in PBS at 37 °C under agitation appears to have a lag phase of ~10 h for a concentration of 2 mg/mL peptide solution. Addition of a small amount of fibril seed (1%, 2%, or 3% (v/v)) to the freshly prepared peptide sample in PBS, in the absence of agitation, induces immediate polymerization, and as a result, the lag phase is essentially eliminated. Notably, the amount of seeding material (1%, 2%, or 3% seed) has different effects on the kinetic behavior: the more seed added, the faster fibrillization occurs (see Figure 5A). The observations that the addition of nucleating seed bypasses the nucleation

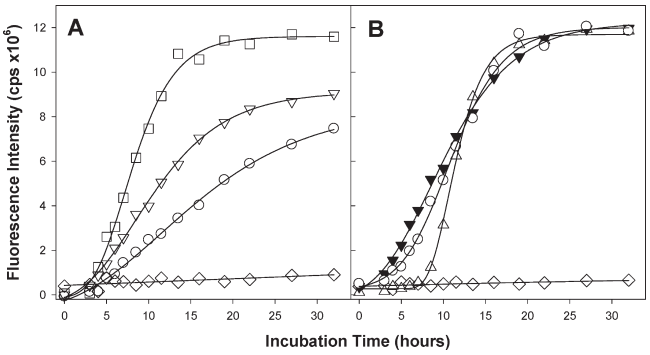

FIGURE 5: Effect of seeding on the kinetics of fibril formation of the PAPf39 peptide monitored by ThT fluorescence. Panel A: 2 mg/mL PAPf39 peptide was incubated in PBS without agitaion at 37 °C in the presence of 1% (circles), 2% (triangles), or 3% (squares) (v/v) preformed fibril seed. PAPf39 peptide in the absence of seed, without agitation (diamonds), served as a control. Panel B: 2 mg/mL PAPf39 peptide was incubated in PBS at 37 °C in the presence of 2% seed without agitation (solid inverted triangles), agitation without seeding (open triangles), both 2% seeding and agitation (open circles), and no seeding or agitation (open diamonds). Solid lines are shown to guide the eye.

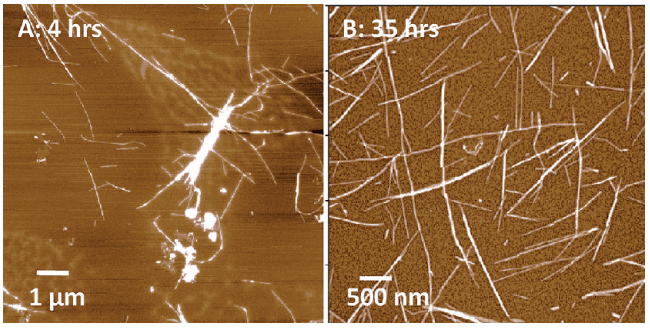

FIGURE 6: Effect of seeding on PAPf39 peptide fibrillization kinetics monitored by AFM. 2 mg/mL PAPf39 peptide was incubated at 37 °C without agitation in the presence of 2% (v/v) preformed fibril seed. Images were taken after 4 h (panel A) and 35 h (panel B). AFM height images were acquired using tapping mode in air.

process (thus shortens or eliminates the lag phase) and that the polymerization rate is seed concentration-dependent are consistent with a nucleation-dependent elongation mechanism for PAPf39 peptide fibril formation. Interestingly, the effects of seeding versus agitation appear to be different. As shown in Figure 5B, agitation alone has a lag phase while seeding alone eliminates the lag phase. However, PAPf39 peptide fibril formation upon agitation occurs at a faster rate during growth phase than fibril formation that occurs as a result of seeding, probably due to agitation-induced fragmentation (*31*). As a result, both samples appear to reach the equilibrium phase at a similar time point. Overall, in accordance with the general nucleation-dependent elongation mechanism, agitation in the presence of seeding eliminates the lag phase and displays the fastest fibril growth (see Figure 5B). The effects of seeding and agitation on PAPf39 peptide fibril formation were further analyzed using AFM. As can be seen from the AFM image of seeded sample after 4 h of incubation at 37 °C (see Figure 6A), both oligomer clusters and fibrils are present. Comparison to the AFM image obtained under agitation conditions (see Figure 4A−C) shows that, at this time point, only spherical oligomers are present. However, 35 h after seeding or after 36 h of agitation long fibrils are observed under both conditions (see Figure 6B and 4H, respectively), in

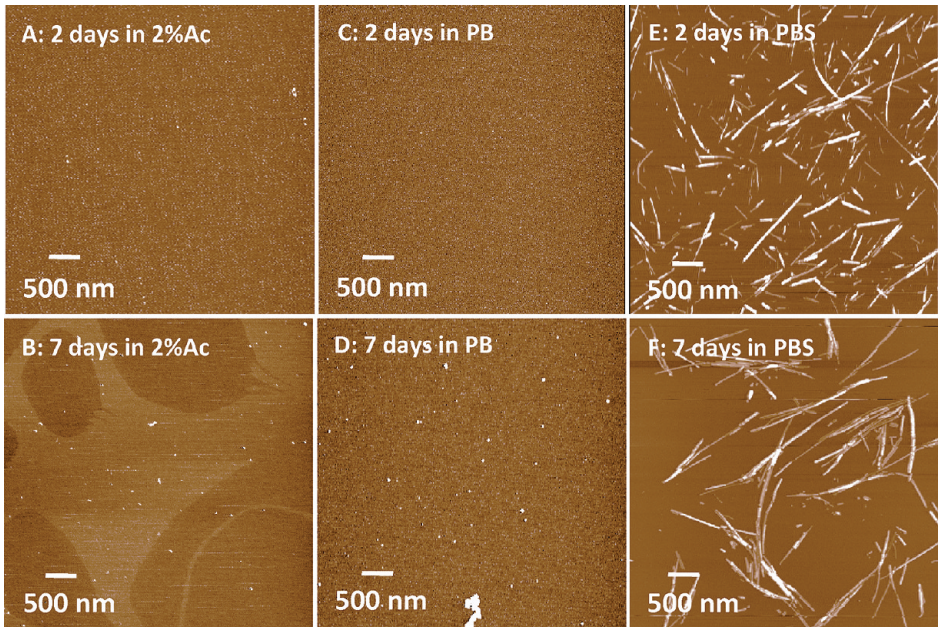

FIGURE 7: Effect of buffers on the aggregation of the PAPf39 peptide monitored by AFM. 2 mg/mL PAPf39 peptide prepared in three different buffers (panels A and B, 2% Ac; panels C and D, PB; panels E and F, PBS) was incubated at 37 °C with agitation for up to 7 days. Images were taken at the time points indicated on the figures. AFM height images were acquired using tapping mode in air.

agreement with ThT experiments (see Figure 5) that by this time point fibrillization is reaching equilibrium phase.

In summary, both AFM analysis and ThT assays suggest that seeding results in faster nucleation but slower elongation of PAPf39 peptide fibrils. Agitation, on the other hand, has a delayed lag phase but promotes fibril growth at a faster rate. This suggests that both seeding and agitation are important factors in the mechanism of PAPf39 peptide fibril formation and may even have somewhat different effects on it. Overall, the kinetics of PAPf39 peptide fibril formation is consistent with a nucleation-dependent fibrillization mechanism.

Role of Charged Residues on PAPf39 Peptide Fibril Formation. PAPf39 peptide is a highly charged molecule with a theoretical pI = 10.2, containing two negatively charged residues (2 Glu), eight positively charged residues (2 Arg and 6 Lys) and two His. The electrostatic interactions among charged residues may be critical in preventing or promoting peptide fibril formation (*2*, *33*). To this end, the effects of three different buffers (low pH, 2% acetic acid; low salt, PB at pH 7.4; high salt, PBS at pH 7.4) on PAPf39 peptide aggregation were compared using a battery of biophysical methods (AFM, ThT fluorescence assays, size exclusion chromatography (SEC), analytical ultracentrifugation (AUC), and small-angle X-ray scattering (SAXS)).

For the AFM imaging, ThT fluorescence assays, and SEC experiments, 2 mg/mL PAPf39 peptide, prepared in these three buffers, was incubated at 37 °C, either with or without agitation, for up to 7 days (~170 h). Aliquots were withdrawn from incubated samples at days 2 and 7 and analyzed by these three methods. It was found that, without agitation, none of the samples formed fibrils, as shown by the above three techniques (data not shown). However, under agitation conditions, different buffers appear to have strikingly different effects on the aggregation profile. As shown by the AFM images in Figure 7A−D, PAPf39 peptide does not form fibrils after 2 or 7 days of incubation in either 2% Ac or PB under agitating conditions, although a small amount of spherical oligomers is visible after 7 days of incubation in both of these solutions. As expected, the peptide in PBS (see Figure 7E,F) forms fibrils after only 2 days of incubation with agitation.

Results from ThT fluorescence assays (see Figure 8A) also demonstrate that only PAPf39 peptide incubated in PBS buffer with agitation gives rise to positive ThT fluorescence, in agreement with fibril formation detected by AFM. Other conditions such as agitation at an acidic pH (i.e., in 2% Ac) or at a neutral pH in the absence of salt (i.e., in PB) do not show a significant increase in ThT fluorescence signals, which suggests that these conditions prevent or slow down fibril formation. Unlike AFM and ThT fluorescence assays, which monitor the presence of amyloid fibrils, SEC detects residual monomeric peptide. Consistent with AFM and ThT fluorescence data, SEC did not show a detectable decrease in the amount of monomer over a time course of 7 days in the sample incubated in 2% Ac, indicating that is does not aggregate at low pH (see Figure 8B). Similarly, the monomer peak only decreases slightly after 7 days for the peptide agitated in PB, suggesting that aggregation is very slow, if any, at physiological pH in the absence of salt. However, the samples agitated in PBS buffer show a dramatic decrease in the monomer concentration after 2 days of incubation and a complete disappearance after 7 days (see Figure 8B).

Equilibrium analytical ultracentrifugation experiments were performed to further investigate the effects of different buffers on the oligomerization state of the PAPf39 peptide. In analytical ultracentrifugation experiments, the distribution of light-absorbing species in the cell depends on the molecular weight of the species and, if any association is taking place, the stoichiometry and equilibrium constant of the association (*34*). Figure 9 shows centrifugation profiles of the PAPf39 peptide in 2% Ac and PB at three different speeds. Samples in PBS precipitated during the course of the experiment, as judged by the continuous decrease in the absorbance, and thus quantitative analysis was not possible. The sedimentation traces for the PAPf39 peptide in 2% Ac were initially fitted to a model of a single ideal species. However, the molecular mass from the fit was much lower than the theoretical molecular mass for the peptide (results not shown), suggesting

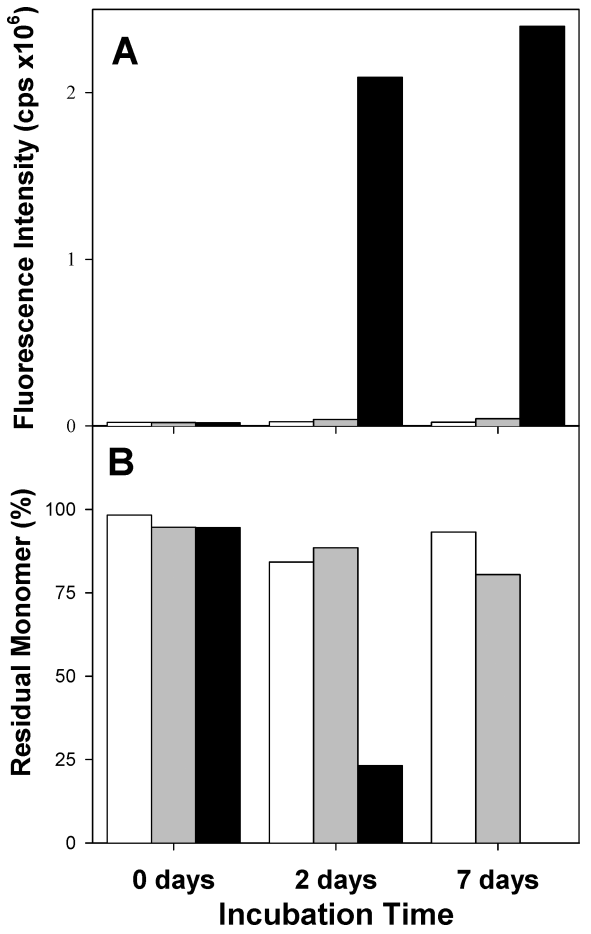

FIGURE 8: Role of charged residues on the aggregation of the PAPf39 peptide monitored by ThT fluorescence and size exclusion chromatography (SEC). 2 mg/mL PAPf39 peptide prepared in three different buffers (2% Ac, open bars; PB, gray bars; PBS, black bars) was incubated at 37 °C with agitation for up to 1 week. At the time points indicated on the *x*-axis, the extent of fibril formation was assayed by ThT fluorescence (panel A), and the fraction of the residual monomers was determined by SEC (panel B).

nonideality, as expected for highly charged molecules. Thus, the traces were analyzed according to a single species model with nonideality (eq 1). The molecular mass obtained from the fit was 4400 ± 200 Da (see Figure 9), which corresponds very well with the theoretical molecular mass of the monomer (4551 Da). The second virial coefficient was positive, 3.8×10^{-5} M, indicating that the peptide has some tendency to self-avoid. The goodness of the fit is demonstrated by the random distribution of the residuals (see Figure 9). The sedimentation traces for the PAPf39 peptide in PB were also fitted according to a single species with nonideality model (see Figure 9) with a reasonably good estimated molecular mass of 4100 ± 300 Da and second virial coefficient of 9×10^{-6} M. However, the distribution of the residuals of the fit is far from random, indicating that under these experimental conditions the model does not fit the experimental profile as well as it does for the data obtained in 2% Ac. In the light of results obtained from AFM image analysis, this is probably due to the presence of some oligomers not in equilibrium with the monomeric species. Nevertheless, the monomeric species appear to represent a dominant fraction of the population.

We used small-angle X-ray scattering to gain some low-resolution structural information about the PAPf39 peptide under two experimental conditions, 2% Ac and PBS. The

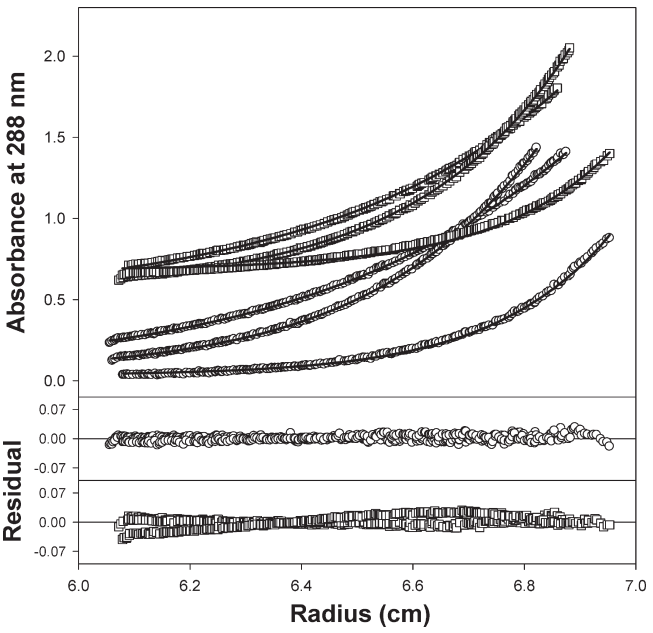

FIGURE 9: Oligomerization state of the PAPf39 peptide in solution monitored by analytical untracentrifugation (AUC). 5 mg/mL PAPf39 peptide was prepared in two different buffers (2% Ac, circles; PB, squares). The samples were spun at 27 °C at three different speeds (28000, 35000, and 40000 rpm). The sedimentation traces for each experimental condition were globally fitted according to eq 1 as described in the text (solid lines). The goodness of the fit is represented by the residuals. The sedimentation profiles for the PAPf39 peptide in PB have been upshifted by 0.5 optical unit for clarity.

experimental scattering profile for the PAPf39 peptide in 2% Ac was analyzed, assuming a monodisperse system, using GNOM software (Figure 10A). The radius of gyration obtained from the fit is $R_g = 18 \pm 1$ Å. This value corresponds very well with the estimated value for a random-coil chain of the same length as PAPf39 peptide (*35*). The shape of the distance distribution function calculated with GNOM (Figure 10C) and the estimates for D_{max} for PAPf39 in 2% Ac (50 Å) are consistent with the dimensions expected for a random-coiled peptide of this length (*36*). The experimental data for the scattering profile of the PAPf39 peptide incubated in PBS were fitted using the GNOM software assuming also a monodisperse system (Figure 10B). The radius of gyration obtained from the fit is $R_g = 160 \pm 5$ Å, indicating that the PAPf39 peptide forms large particles under these conditions. The distance distribution function for the PAPf39 peptide in PBS calculated with GNOM (Figure 10C) is also very different from the one for the PAPf39 peptide in 2% Ac, which is consistent with a significant structural change occurring during incubation in PBS. The D_{max} for the PAPf39 peptide in PBS is ~530 Å, in agreement with the fibrillar structures observed in AFM images. Assuming in a first approximation that the species in 2% Ac and PBS are both spherical structures with the same density and knowing that the species in 2% Ac are PAPf39 monomers, we can estimate the average number of monomers per fibril formed during incubation of the PAPf39 peptide in PBS as $N = R_g(\text{PBS})^3/R_g(2\%\ \text{Ac})^3 \approx 700$. This is most likely the lowest possible stochiometry of monomers in the assembly, since fibrillar structures are probably more dense than the PAPf39 peptide monomers. All of these results are fully consistent with the results of AFM (Figure 7) and ThT fluorescence and AUC experiments (Figure 8).

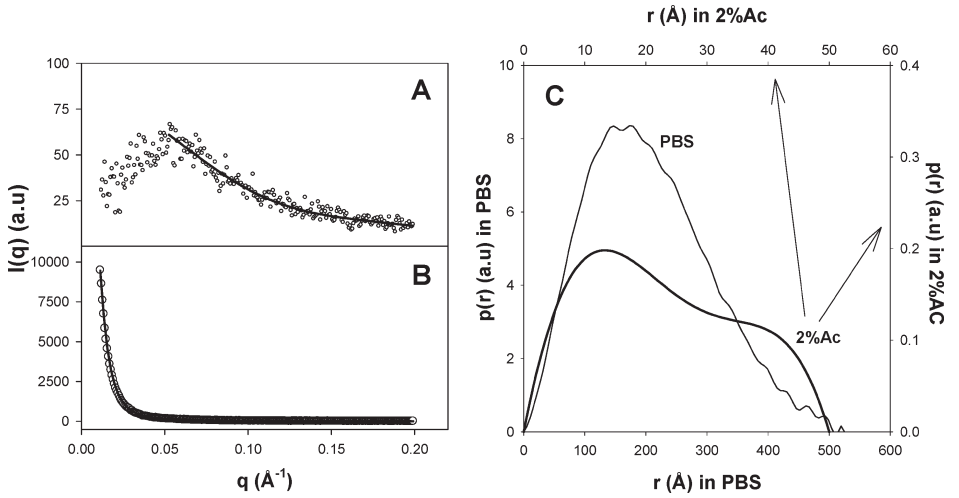

FIGURE 10: Small angle X-ray scattering profiles for the PAPf39 peptide. Experimental scattering profiles (symbols) and fit (continuous line) computed by GNOM assuming a monodisperse system for the PAf39 peptide in 2% Ac (panel A) and in PBS (panel B). Panel C: Distance distribution function computed by GNOM from the experimental data in 2% Ac and PBS shown in panels A and B.

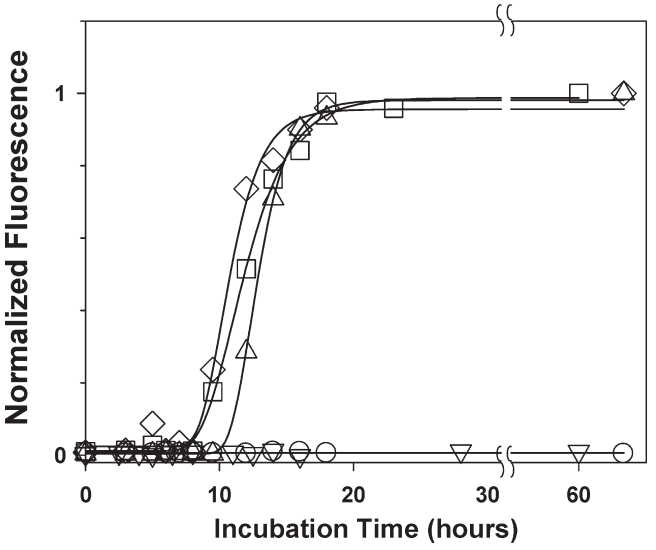

FIGURE 11: Effect of salt on the aggregation of the PAPf39 peptide monitored by ThT fluorescence. 2 mg/mL PAPf39 peptide was prepared in PB at different NaCl concentrations (0 mM, circles; 50 mM, inverted triangles; 100 mM, squares; 150 mM, diamonds; 300 mM, triangles) and incubated at 37 °C with agitation for up to 3 days. At different time points, samples were assayed by ThT fluorescence. Solid lines are shown to guide the eye.

To summarize, PAPf39 peptide does not self-assemble into amyloid fibrils in PB (low salt, pH 7.4) or acetic acid (low pH) solutions, even under agitation conditions. In contrast, PAPf39 peptide in PBS (high salt, pH 7.4) readily forms fibrils upon agitation, suggesting that not only pH but the presence of salt is critical in PAPf39 peptide fibril formation. As shown above, the PAPf39 peptide forms amyloid fibrils in PBS but not in PB at neutral pH under agitation conditions. This prompted us to further investigate the effect of salt on PAPf39 peptide fibril formation. To this end, fresh peptides prepared in 20 mM PB buffer (pH 7.4) in the presence of different concentrations of salt (at 0, 50, 100, 150, and 300 mM NaCl) were incubated at 37 °C with agitation for up to 3 days (72 h). The kinetics of fibrillization was monitored by a ThT fluorescence assay. As illustrated in Figure 11, in the absence of salt or in the presence of low concentration of salt, i.e., 50 mM NaCl, fibril formation is not observed under agitating conditions. In contrast, when the salt concentration was increased to 100 mM or higher, the kinetics profile changed dramatically, and the fibrillization process was observed. Interestingly, the aggregation kinetics is similar at 100, 150, or 300 mM NaCl concentrations (Figure 11). Thus, it is clear that electrostatic interactions between charged residues play an important role in PAPf39 peptide fibril formation. The inhibition of fibril formation at low pH may be due to the protonation of the two His residues in the PAPf39 peptide sequence and/or neutralization of the two carboxylic acids of the Glu side chains. The effects of salt are more difficult to rationalize without more detailed information on the structure of the conformational ensemble of the monomeric peptide and the structure of the PAPf39 fibrils.

CONCLUSIONS

The kinetics of PAPf39 peptide fibrillization was studied by different biophysical methods (ThT fluorescence assays, AFM, SEC, SAXS, AUC) and shown to follow a nucleation-dependent elongation mechanism. Several critical factors for fibrillization have been identified. It was shown that agitation and/or seeding seem(s) to be required for fibril formation at 37 °C and neutral pH, with an additional requirement of a salt concentration above ~100 mM. Fibril formation by the PAPf39 peptide is inhibited by low pH or by low salt concentration at neutral pH. These observations suggest that nucleation and fibrillization of the PAPf39 peptide are a tug-of-war between the interactions formed upon agitation and the electrostatic interactions, modulated by pH and salt concentration.

ACKNOWLEDGMENT

We thank Analytical, Imaging, and Macromolecular Cores at the Center for Biotechnology and Interdisciplinary Studies for providing accessibility to fluorescence spectroscopy, small angle X-ray scattering, and the atomic force microscope.

REFERENCES

1. Dobson, C. M. (1999) Protein misfolding, evolution and disease. *Trends Biochem. Sci. 24*, 329–332.
2. Chiti, F., and Dobson, C. M. (2006) Protein misfolding, functional amyloid, and human disease. *Annu. Rev. Biochem. 75*, 333–366.

3. Goto, Y., Yagi, H., Yamaguchi, K., Chatani, E., and Ban, T. (2008) Structure, formation and propagation of amyloid fibrils. *Curr. Pharm. Des. 14*, 3205–3218.
4. Guijarro, J. I., Sunde, M., Jones, J. A., Campbell, I. D., and Dobson, C. M. (1998) Amyloid fibril formation by an SH3 domain. *Proc. Natl. Acad. Sci. U.S.A. 95*, 4224–4228.
5. Bucciantini, M., Giannoni, E., Chiti, F., Baroni, F., Formigli, L., Zurdo, J., Taddei, N., Ramponi, G., Dobson, C. M., and Stefani, M. (2002) Inherent toxicity of aggregates implies a common mechanism for protein misfolding diseases. *Nature 416*, 507–511.
6. Chiti, F., Webster, P., Taddei, N., Clark, A., Stefani, M., Ramponi, G., and Dobson, C. M. (1999) Designing conditions for in vitro formation of amyloid protofilaments and fibrils. *Proc. Natl. Acad. Sci. U.S.A. 96*, 3590–3594.
7. Damaschun, G., Damaschun, H., Gast, K., and Zirwer, D. (1999) Proteins can adopt totally different folded conformations. *J. Mol. Biol. 291*, 715–725.
8. Krebs, M. R., Wilkins, D. K., Chung, E. W., Pitkeathly, M. C., Chamberlain, A. K., Zurdo, J., Robinson, C. V., and Dobson, C. M. (2000) Formation and seeding of amyloid fibrils from wild-type hen lysozyme and a peptide fragment from the beta-domain. *J. Mol. Biol. 300*, 541–549.
9. Rochet, J. C., and Lansbury, P. T., Jr. (2000) Amyloid fibrillogenesis: themes and variations. *Curr. Opin. Struct. Biol. 10*, 60–68.
10. Sunde, M., and Blake, C. (1997) The structure of amyloid fibrils by electron microscopy and X-ray diffraction. *Adv. Protein Chem. 50*, 123–159.
11. Glenner, G. G. (1981) The bases of the staining of amyloid fibers: their physico-chemical nature and the mechanism of their dye-substrate interaction. *Prog. Histochem. Cytochem. 13*, 1–37.
12. Naiki, H., Higuchi, K., Hosokawa, M., and Takeda, T. (1989) Fluorometric determination of amyloid fibrils in vitro using the fluorescent dye, thioflavin T1. *Anal. Biochem. 177*, 244–249.
13. Harper, J. D., and Lansbury, P. T., Jr. (1997) Models of amyloid seeding in Alzheimer's disease and scrapie: mechanistic truths and physiological consequences of the time-dependent solubility of amyloid proteins. *Annu. Rev. Biochem. 66*, 385–407.
14. Munch, J., Rucker, E., Standker, L., Adermann, K., Goffinet, C., Schindler, M., Wildum, S., Chinnadurai, R., Rajan, D., Specht, A., Gimenez-Gallego, G., Sanchez, P. C., Fowler, D. M., Koulov, A., Kelly, J. W., Mothes, W., Grivel, J. C., Margolis, L., Keppler, O. T., Forssmann, W. G., and Kirchhoff, F. (2007) Semen-derived amyloid fibrils drastically enhance HIV infection. *Cell 131*, 1059–1071.
15. Lednev, I. K., Ermolenkov, V. V., He, W., and Xu, M. (2005) Deep-UV Raman spectrometer tunable between 193 and 205 nm for structural characterization of proteins. *Anal. Bioanal. Chem. 381*, 431–437.
16. Makhatadze, G. I., Medvedkin, V. N., and Privalov, P. L. (1990) Partial molar volumes of polypeptides and their constituent groups in aqueous solution over a broad temperature range. *Biopolymers 30*, 1001–1010.
17. Svergun, D. I. (1992) Determination of the regularization parameter in indirect-transform methods using perceptual criteria. *J. Appl. Crystallogr. 25*, 495–503.
18. Naiki, H., Higuchi, K., Matsushima, K., Shimada, A., Chen, W. H., Hosokawa, M., and Takeda, T. (1990) Fluorometric examination of tissue amyloid fibrils in murine senile amyloidosis: use of the fluorescent indicator, thioflavine T. *Lab. Invest. 62*, 768–773.
19. Gosal, W. S., Myers, S. L., Radford, S. E., and Thomson, N. H. (2006) Amyloid under the atomic force microscope. *Protein Pept. Lett. 13*, 261–270.
20. Conway, K. A., Lee, S. J., Rochet, J. C., Ding, T. T., Williamson, R. E., and Lansbury, P. T., Jr. (2000) Acceleration of oligomerization, not fibrillization, is a shared property of both alpha-synuclein mutations linked to early-onset Parkinson's disease: implications for pathogenesis and therapy. *Proc. Natl. Acad. Sci. U.S.A. 97*, 571–576.
21. Chromy, B. A., Nowak, R. J., Lambert, M. P., Viola, K. L., Chang, L., Velasco, P. T., Jones, B. W., Fernandez, S. J., Lacor, P. N., Horowitz, P., Finch, C. E., Krafft, G. A., and Klein, W. L. (2003) Self-assembly of Abeta(1−42) into globular neurotoxins. *Biochemistry 42*, 12749–12760.
22. Harper, J. D., Lieber, C. M., and Lansbury, P. T., Jr. (1997) Atomic force microscopic imaging of seeded fibril formation and fibril branching by the Alzheimer's disease amyloid-beta protein. *Chem. Biol. 4*, 951–959.
23. Lashuel, H. A., and Lansbury, P. T., Jr. (2006) Are amyloid diseases caused by protein aggregates that mimic bacterial pore-forming toxins? *Q. Rev. Biophys. 39*, 167–201.
24. Quist, A., Doudevski, I., Lin, H., Azimova, R., Ng, D., Frangione, B., Kagan, B., Ghiso, J., and Lal, R. (2005) Amyloid ion channels: a common structural link for protein-misfolding disease. *Proc. Natl. Acad. Sci. U.S.A. 102*, 10427–10432.
25. Johnson, W. C., Jr. (1990) Protein secondary structure and circular dichroism: a practical guide. *Proteins 7*, 205–214.
26. Xu, M., Shashilov, V., and Lednev, I. K. (2007) Probing the cross-beta core structure of amyloid fibrils by hydrogen-deuterium exchange deep ultraviolet resonance Raman spectroscopy. *J. Am. Chem. Soc. 129*, 11002–11003.
27. Huang, C. Y., Balakrishnan, G., and Spiro, T. G. (2006) Protein secondary structure from deep-UV resonance Raman spectroscopy. *J. Raman Spectrosc. 37*, 277–282.
28. Englander, S. W., Sosnick, T. R., Englander, J. J., and Mayne, L. (1996) Mechanisms and uses of hydrogen exchange. *Curr. Opin. Struct. Biol. 6*, 18–23.
29. Lazo, N. D., Grant, M. A., Condron, M. C., Rigby, A. C., and Teplow, D. B. (2005) On the nucleation of amyloid beta-protein monomer folding. *Protein Sci. 14*, 1581–1596.
30. Roan, N. R., Munch, J., Arhel, N., Mothes, W., Neidleman, J., Kobayashi, A., Smith-McCune, K., Kirchhoff, F., and Greene, W. C. (2009) The cationic properties of SEVI underlie its ability to enhance human immunodeficiency virus infection. *J. Virol. 83*, 73–80.
31. Xue, W. F., Homans, S. W., and Radford, S. E. (2008) Systematic analysis of nucleation-dependent polymerization reveals new insights into the mechanism of amyloid self-assembly. *Proc. Natl. Acad. Sci. U.S.A. 105*, 8926–8931.
32. Nielsen, L., Khurana, R., Coats, A., Frokjaer, S., Brange, J., Vyas, S., Uversky, V. N., and Fink, A. L. (2001) Effect of environmental factors on the kinetics of insulin fibril formation: elucidation of the molecular mechanism. *Biochemistry 40*, 6036–6046.
33. Ma, K., Clancy, E. L., Zhang, Y. B., Ray, D. G., Wollenberg, K., and Zagorski, M. G. (1999) Residue-specific pK(a) measurements of the beta-peptide and mechanism of pH-induced amyloid formation. *J. Am. Chem. Soc. 121*, 8698–8706.
34. Laue, T. M., and Stafford, W. F., III (1999) Modern applications of analytical ultracentrifugation. *Annu. Rev. Biophys. Biomol. Struct. 28*, 75–100.
35. Fitzkee, N. C., and Rose, G. D. (2004) Reassessing random-coil statistics in unfolded proteins. *Proc. Natl. Acad. Sci. U.S.A. 101*, 12497–12502.
36. Tran, H. T., Wang, X., and Pappu, R. V. (2005) Reconciling observations of sequence-specific conformational propensities with the generic polymeric behavior of denatured proteins. *Biochemistry 44*, 11369–11380.
37. Huang, C. Y., Balakrishnan, G., and Spiro, T. G. (2005) Early events in apomyoglobin unfolding probed by laser T-jump/UV resonance Raman spectroscopy. *Biochemistry 44*, 15734–15742.